IIT, Madras

Topology optimization of the hip bone for a few activities of daily living

Kandula Eswara Sai Kumar[1] · Sourav Rakshit[1]

Abstract Hip bone is a robust and complex skeletal structure in the human body and it bears loads while doing the daily activities such as walking, running, etc., by connecting the leg with the torso. The geometry of the hip bone facilitates upright gait in humans and hence its evolution might have been influenced by the mechanical forces acting on it. Previous research works on hip bone mainly concentrated upon its analysis using methods like finite elements. However, no work is reported on the geometric optimization of the hip bone, i.e., how optimal is the geometry of the hip bone under mechanical loads of activities of daily living (ADL). Hence, in this work we explore the optimal geometry of the hip bone during two ADLs, walking, and sit-to-stand. This is posed as the topology optimization problem of compliance minimization of the hip bone under mechanical loads of walking and sit-to-stand. With a view to applications in prosthesis and hemiarthroplasty, we impose equality in volume constraint as the natural hip bone, and guide the optimal designs to generate the hole (obturator foramen in the natural hip bone) in the optimal designs. This is done by using a designer guided approach that consists of a two-step optimization procedure: first selecting results from topology optimization for a particular activity that give high shape similarity with natural hip bone, and then using it as input to topology optimization with loads from the other activity, for example, applying sit-to-stand loads on optimal design from walking. We demonstrate that this designer guided approach leads to exploration of the design space with a reduced set of inputs and increase in shape similarity of the final design with the natural hip bone.

Keywords Biomechanics · Walking · Sit-to-stand · OptiStruct® · OpenSim

1 Introduction

Hip bone is a robust and complex structure in the human body and transfers mechanical loads from the upper body (head, hands, and torso) to lower body (legs) as the body does activities like standing, walking, running, sit-to-stand, etc. It is a part of pelvic girdle and consists of three bones: the ilium, the ischium and the pubis bone. These three bones are fused together at the acetabulum (where thigh bone is connected to the hip bone). The hip bone has a hole between the ischium bone and the pubis bone, called the obturator foramen, through which blood vessels and nerves pass. This hole creates stress concentrations, and among the most common modes of hip fracture, the lateral compression and vertical shear fracture modes occur in bones surrounding the obturator foramen [1]. Hence, we are motivated to pose the following design question: are there similar geometric structures as the hip bone bearing the same loads under same boundary conditions, but more stiff (implying less chances of fracture) than the natural hip bone? The structural similarity might be essential for maintaining the functions of the hip bone like upright bipedal gait and providing bone marrow for generation of blood cells. Till now, no work is reported on the optimal design of hip prosthesis considering the effect of loads of ADLs, or bio-functional aspects like presence of muscle attachment sites. Hence, there is a need for the design of a

✉ Sourav Rakshit
srakshit@iitm.ac.in

1 Machine Design Section, Department of Mechanical Engineering, IIT Madras, Chennai, Tamil Nadu 600036, India

prosthesis that maintains the same functions as the natural hip bone and structurally stronger than the natural hip bone.

Deformation study of the hip bone under loads of various activities like walking and running is a well-studied area of research. Finite element (FE) analysis has been widely and almost exclusively used to analyze the complex sandwich structure of the hip bone under mechanical loads. Various 3D FE models have been used to do realistic analysis of the sandwich material comprising the hip bone, i.e., the trabecular bone covered by a layer of cortical shell for walking loads. Goel et al. [2, 3] made the first attempts to calculate stresses in the pelvis and hip bone using a FE model. Dostal and Andrews [4] formulated a straight-line model to estimate muscle forces from elastic strings connected between hip bone and femur. Bergmann et al. [5] measured the resultant hip joint force, its orientation and moments during walking and running from patients using telemetering total hip prosthesis. Dalstra and Huiskes [6] calculated the muscle forces during eight phases of gait cycle and found that maximum stress occurs during one legged stance phase. They also noted high stresses in the outer cortical shell than in the inner trabecular matrix of the hip bone. Anderson et al. [7] developed a patient specific model of pelvis and carried out validation and sensitivity studies using FE. Ghosh et al [8] investigated the variation in load transfer due to fixing an implant. Ghosh et al. [9] investigated the changes in acetabular stresses and strains due to the inclusion of cartilage layer at the hip joint using a 3D FE model. Mukherjee and Gupta [10] developed a framework to understand progressive tissue differentiation and bone ingrowth around the acetabular component. Hu et al. [11] explored the effect of boundary conditions on load transmission to the pelvic bone by using FE analysis. They suggested that determination of boundary and connection conditions have to be modeled more closely to existing bone to study the clinical applications. Ricci et al. [12] investigated the distribution of force in the pelvic ring for the mechanical loads of a gait cycle. Ramezani et al. [13] refined an existing FE model of the pelvis with the help of in vitro data of load and deformation by using an inverted validation approach.

Sit-to-stand is defined as moving the mass center of body upward from sitting to standing position. Sit-to-stand has a consistent pattern of forward lean followed by a lift to reach the standing position [14]. In contrast to walking, only a few studies have been performed to understand the kinematics of the sit-to-stand. Kotake et al. [15] analyzed the movements involved in sit-to-stand and observed regular series of transition points in the angles of joints (hip, knee and ankle). Mourey et al. [16] compared the center of mass control in young and elderly people during the sit-to-stand. Janssen et al. [17] identified the determinants of the

sit-to-stand and described their effect on the performance of sit-to-stand. Yoshioka et al. [18] examined the effect of seat height on maximum joint force and moments of lower limbs during sit-to-stand. Carthers et al. [19] developed an OpenSim model to examine the influence of muscle forces on the horizontal and vertical acceleration of the center of mass during sit-to-stand. Tse et al. [20] evaluated the pelvic response for underbody blast (UBB) for different seating positions and suggested that upright seated posture may have low risk of pelvic injuries under UBB.

On the other hand, bone micro-structure design using methods like topology optimization is an area of active research [21–24]. However, most of these researches have focused on developing bone micro-structural models of the femur bone where the global geometry of the bone is fixed. Thus, we see a research gap for an attempt towards designing the global geometry of a load bearing bone. Hip bone is such a bone; it bears considerable mechanical loads during movement of the body (the whole weight of upper part of the body is transmitted to the legs through the hip bone, and similarly all forces from the femur is transmitted to the upper body through it), and has sufficient complicated geometry (upper part flat and lower part undulated with a hole in middle) of genus one. Thus, the optimal design of the global geometry of the hip bone under mechanical loads of different ADLs is a problem worth challenging and has not received much attention. Recently, Kumar and Rakshit [25, 26] presented the optimal design of hip bone for walking loads, and the design of hip bone prosthesis under single leg stance [27].

In this work, we present the optimal design of the hip bone for two ADLs, walking, and sit-to-stand. The particular focus of this work is the user guided design of the hip bone by using combination of the loads of walking and sit-to-stand. The design approach in 'combination of phases' presented in [27] is extended to inter-combination of phases between walking and sit-to-stand. Rest of the paper is organized as follows: Sect. 2 explains topology optimization and its sensitivity analysis. It also introduces the two ADLs that we consider for topology optimization, Procrustes analysis and a user-guided design approach for solving combination between walking and sit-to-stand. Section 3 presents the optimal design of the hip bone for walking, sit-to-stand and combination between walking and sit-to-stand. Section 4 concludes with final remarks and future work.

2 Methods

2.1 Topology optimization

Topology optimization (TO) finds the optimal material distribution of a structure for a given objective function with the constraints. Generally, the objective functions in TO of solid structures are: compliance minimization, frequency maximization, design synthesis for specified force/displacement. Compliance minimization with volume constraint has been widely used for stiff structure design with volume constraints [28]. The compliance minimization formulation is given as:

$$
\begin{aligned}
\text{minimize:} \quad & \int_{\Gamma} s_i u_i \mathrm{d}\Gamma \\
\text{Subject to:} \quad & \int_{\Omega} \rho \mathrm{d}\Omega - V_{\max} \leq 0 \\
& \text{div}(C_{ijkl} u_{k,l}) = 0 \quad \text{on} \quad \Omega \\
& u_i = \bar{u}_0 \quad \text{on} \quad \Gamma_u \\
& s_i = \bar{s}_0 \quad \text{on} \quad \Gamma_s \\
& 0 \leq \rho \leq 1
\end{aligned}
\tag{1}
$$

where s_i is the traction, u_i is the displacement, ρ is the non-dimensional density (design variable) and varies from 0 (void material) to 1 (solid material), $V_{\max}$ is the maximum allowable volume, C_{ijkl} is the elastic tensor, Ω is the design domain, Γ is the boundary of the domain, Γ_u is the displacement boundary and Γ_s is the force boundary. Using a numerical method like finite element the above formulation can be posed as:

$$
\begin{aligned}
\text{minimize:} \quad & c = \mathbf{f}^{\mathrm{T}} \mathbf{u} \\
\text{Subject to:} \quad & V \leq V_{\max} \\
& \mathbf{K}\mathbf{u} = \mathbf{f}
\end{aligned}
\tag{2}
$$

where c, the compliance of a structure is defined as the work done by external forces on the structure, $\mathbf{K}$ is the stiffness matrix, $\mathbf{u}$ is the displacement vector, $\mathbf{f}$ is the force vector and V is the volume of the structure that should not be greater than the maximum allowable volume $V_{\max}$. In this problem, we considered $V_{\max}$ as the enclosed volume of the hip bone.

2.1.1 Sensitivity analysis

The modified elemental stiffness matrix using a material modeling technique like Solid Isotropic Material Penalization (SIMP) method is given as:

$$
\begin{aligned}
& \mathbf{k}_e = \rho^p \mathbf{k}_0, \\
& 0 < \rho_{\min} \leq \rho \leq 1
\end{aligned}
\tag{3}
$$

where ρ is the design variable, $\mathbf{k}_e$ is the modified elemental stiffness matrix, $\mathbf{k}_0$ is the initial elemental stiffness matrix, p is the penalization factor (greater than 1, usually 3) and $\rho_{\min} (= 0.001)$ is the lower limit on the design variable to avoid singularity [29, 30]. The objective function using SIMP method is given as:

$$
\begin{aligned}
c_e &= \mathbf{f}_e^{\mathrm{T}} \mathbf{u}_e \\
&= \mathbf{u}_e^T \mathbf{k}_e \mathbf{u}_e \\
&= \rho^p \mathbf{u}_e^T \mathbf{k}_0 \mathbf{u}_e
\end{aligned}
\tag{4}
$$

where the subscript e represents an elemental quantity. Since many of the established topology optimization algorithms use gradient-based optimization methods, sensitivities of the objective function and the constraints are required. The sensitivity of elemental compliance c_e with respect to the design variable density (ρ) is defined as:

$$
\begin{aligned}
\frac{\partial c_e}{\partial \rho} &= -\frac{\partial}{\partial \rho} (\mathbf{f}_e^T \mathbf{u}_e) \\
&= -\frac{\partial}{\partial \rho} (\mathbf{u}_e^T \mathbf{k}_e \mathbf{u}_e)
\end{aligned}
\tag{5}
$$

From Eqs. 3–5, the analytical expression for sensitivity of the objective function (compliance) with respect to the design variable (ρ) is given as:

$$
\frac{\partial c_e}{\partial \rho} = -p\rho^{p-1} \mathbf{u}_e^T \mathbf{k}_0 \mathbf{u}_e.
\tag{6}
$$

2.1.2 Design and non-design domains

In general TO starts with an arbitrary design domain and optimizes it based on the objective function but this work uses a highly constrained domain due to the presence of boundary conditions. If initial input to topology optimization is any general primitive shape like cubiod; then following difficulties are faced:

- Modeling the muscle attachment areas inside the cuboid involves the modeling of the replica surface of these muscle attachment areas; this increases the complexity of modeling; and meshing of these complex modeled areas is difficult.
- The application of traction boundary conditions on inner elements is not allowed. The inner elements can take only body forces, while the boundary elements can take traction.
- To avoid the convergence to a local optimal solution since OptiStruct® solver uses a convex optimization technique.

The following are list of boundary conditions acting on the hip bone:

- Fixed boundary conditions at pubic symphysis (joint between two hip bones) and sacro-iliac joint (joint

between the hip bone and lower part of the spinal chord).

- Hip joint forces at acetabulum (joint between the hip bone and the femur/thigh bone).
- Muscle attachment areas through which muscles apply active force on the hip bone.

The input design domain after considering all these boundary conditions is shown in Fig. 2. It has similar outer geometry as natural hip bone but the design domain and natural hip bone is topologically different since the natural hip bone has a hole. In this work, we use non-design domains to prevent material removal from the unwanted areas. These are listed as:

- Iliac crest is a bone marrow rich region which generates new blood cells.
- Muscle attachment areas provide connection to muscles that apply forces on the hip bone.

These areas are included into non-design domains to maintain the biological functionality of the hip bone [26].

2.2 Modeling of the hip bone

This work uses the hip bone geometric model which is purchased from TurboSquid domain. It is built from a 3D laser scanner with 0.1 mm accuracy using laser topography (LT) technique. The solid geometry is defined with the help of a surface triangular mesh which is obtained from the LT point cloud.

Each hip bone is connected to sacrum at sacro-iliac joint, other hip bone at pubic symphysis and the femur at acetubulum (Fig. 1). The deformation of the sacro-iliac joint and pubic symphysis are negligible when compared with the acetabulum, hence the pubic symphysis and the sacro-iliac joint are fixed and the hip joint force is applied at acetabulum [7]. Hip bone is connected to 21 muscles which apply active forces during various ADLs through the muscle attachment areas. Hence, we include the muscle forces in the force boundary conditions and the magnitude of the muscle forces are either adopted from the literature or obtained from OpenSim software.

2.3 Activities of daily living (ADLs)

2.3.1 Walking

The walking gait cycle is divided into eight phases as shown in Fig. 3. The magnitude of the hip joint force and muscle forces for a person of body weight of 650 N during walking gait cycle is presented in Tables 1 and 2,
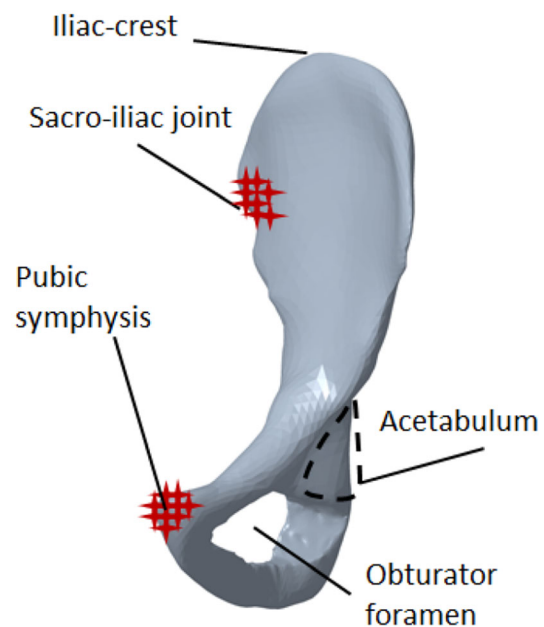

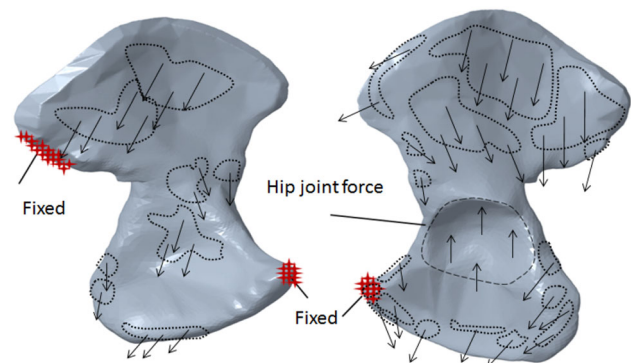**Fig. 1** Natural hip bone with its components and the boundary conditions

Fig. 2 Design domain with the boundary conditions

respectively, and are adopted from Dalstra and Huiskes [6]. The coordinate data for proximal and distal points of muscle are presented by Dostal and Andrews [4] are used in this work to find out the muscle directions.

2.3.2 Sit-to-stand

The sit-to-stand is divided into five phases as shown in Fig. 4. We use OpenSim software to obtain the muscle forces acting on the hip bone for sit-to-stand. We use the model presented by Caruthers et al. [19] to calculate the
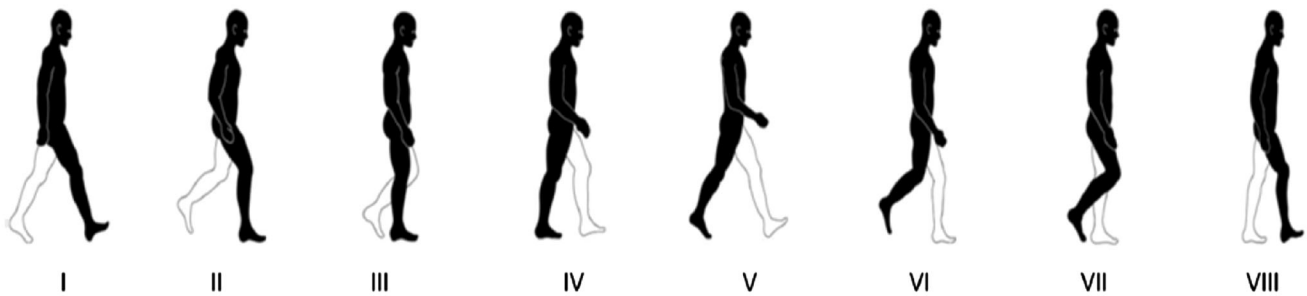
Fig. 3 Eight phases of walking gait cycle [25]

Table 1 Description of load phases and hip joint forces during a gait cycle for a human of weight 650 N [6]

Phase	Description	Occurrence in gait cycle (%)	Hip joint force (N)
I	Beginning stance phase	2	426
II	Beginning support phase	13	2158
III	Halfway support phase	35	1876
IV	End support phase	48	1651
V	End stance phase	52	1180
VI	Beginning swing phase	63	187
VII	Halfway swing phase	85	87
VIII	End swing phase	98	379

muscle forces for sit-to-stand. The direction of the muscle forces is obtained from the 'MuscleForceDirection' plugin in OpenSim [31, 32]. The hip joint force for sit-to-stand is adopted from Yoshioka et al. [18]. The description of the load phases and corresponding hip joint forces during sit-to-stand for a human of weight 650 N is presented in Table 3. Table 4 lists the muscle forces for the five phases of the sit-to-stand for a human of weight 650 N [19].

This work uses the finite element model of the hip bone from our previous work Kumar and Rakshit [25], which is validated against literature.

2.4 Procrustes analysis

Procrustes analysis (PA) is a technique to find the shape similarity between two shapes using coordinate data. PA removes translation, scaling and rotation components from either of the coordinate data to produce the transformed data. The normalized sum of squared distance between the transformed data and other coordinate data gives the dissimilarity index (D). The similarity index (S) is defined as:

$$S = 1 - D. \tag{7}$$

2.5 Combination between walking and sit-to-stand

This section describes a method that uses the shape similarity values for a user-guided design of the hip bone. The method follows closely the approach presented in [25], however, in this work we extend it to two ADLs, walking and sit-to-stand. To understand our approach, let the walking phases be denoted by the set $S_1 = \{I, II, III, IV, V, VI, VII, VIII\}$ and sit-to-stand phases be denoted by the set $S_2 = \{A, B, C, D, E\}$. The problem is to determine how many permutations exist without any repetition. Each permutation denotes a sequence of user guided optimization procedure. For example, the permutation $I - A - II - B$ implies the following design procedure: on optimal design (D_1 say) from loading conditions of I use loading conditions of A to get a new optimal design (D_2 say), then use loading condition II on D_2 to get the optimal design D_3, and then get the final design D_4 by applying loading condition B on D_3. There can be different ways of determining the permutations. If elements of S_1 and S_2 are chosen indiscriminately, then total number of permutations is $13! = 6227020800$. One may wish to reduce the number of permutations by choosing to apply elements of S_1 and S_2 alternatively. This gives $2 \times 8! \times 5! = 9676800$ permutations (the 2 is for selecting either of S_1 or S_2 first). However, this also gives a very high number of permutations. As we will show later, the designer can reduce the number

Table 2 Muscle forces on hip bone during eight phases of gait cycle for a human of weight 650 N [6]

S. no.	Muscle name	Forces (N) during eight phases of gait cycle							
		P1	P2	P3	P4	P5	P6	P7	P8
1	Tensor fascia latae	0	132	88	158	149	88	70	96
2	Sartorius	0	88	0	0	35	158	88	88
3	Rectus femoris	0	123	0	0	0	175	105	96
4	Pectineus	0	0	175	96	0	149	0	0
5	Adductor longus	0	88	0	0	88	158	70	140
6	Gracilis	0	0	0	0	88	158	70	140
7	Adductor brevis	0	114	0	0	0	202	0	114
8	Adductor magnus	0	0	0	0	132	263	0	0
9	Obturator externus	0	0	0	0	123	167	132	123
10	Quadratus femoris	61	96	0	0	88	184	0	0
11	Semimembranosus	579	368	333	368	421	298	61	421
12	Gemellus superior	140	88	123	79	0	0	158	202
13	Piriformis	202	275	0	0	0	0	123	228
14	Psoas	149	0	316	175	88	175	105	140
15	Obturator internus	167	123	0	61	61	149	123	0
16	Semitendinosus	0	140	105	246	316	368	105	0
17	Gemellus inferior	0	0	0	0	0	140	79	149
18	Iliacus	0	0	0	228	307	272	0	0
19	Gluteus minimus	228	140	263	228	175	123	114	219
20	Gluteus medius	1018	1053	1474	1509	1412	982	105	421
21	Gluteus maximus	842	930	167	377	456	491	114	482

P1–P8 represents the eight phases of gait cycle

Fig. 4 Five phases of sit-to-stand [19]

I   II   III   IV   V
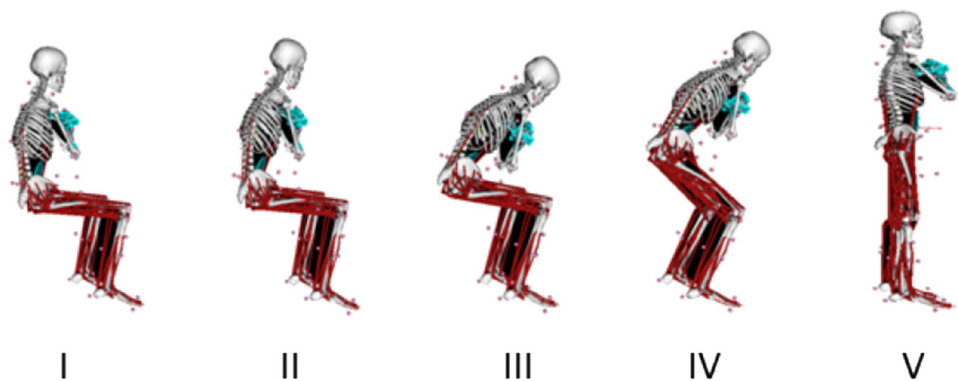
Table 3 Description of load phases and hip joint forces during sit-to-stand for a human of weight 650 N [18]

Phase	Description	Occurrence in gait cycle (%)	Hip joint force (N)
I	Beginning of the STS	5	1594
II	Forward Leaning	29	1297
III	Momentum transfer	38	950
IV	Extension	61	608
V	Ending of the STS	81	355

Table 4 Forces on hip bone during five phases of sit-to-stand for a human of weight 650 N [19]

S. no.	Muscle name	Forces (N) during five phases of gait cycle				
		P1	P2	P3	P4	P5
1	Tensor fascia latae	15	0	0	12	121
2	Sartorius	155	124	152	156	113
3	Rectus femoris	1250	993	990	1242	509
4	Pectineus	65	0	130	51	150
5	Adductor longus	41	62	0	37	456
6	Gracilis	96	67	0	65	112
7	Adductor brevis	31	56	66	146	301
8	Adductor magnus	415	364	510	642	667
9	Obturator externus	0	0	0	0	0
10	Quadratus femoris	146	117	200	78	92
11	Semimembranosus	117	0	26	292	373
12	Gemellus superior	50	0	19	44	46
13	Piriformis	42	0	8	100	87
14	Psoas	507	228	537	513	523
15	Obturator internus	0	0	0	0	0
16	Semitendinosus	93	4	21	144	173
17	Gemellus inferior	50	0	19	44	46
18	Iliacus	62	0	10	113	733
19	Gluteus minimus	43	0	11	144	368
20	Gluteus medius	91	0	20	435	1104
21	Gluteus maximus	618	1316	283	24	373

of permutations by only choosing a small number of optimal designs that have high shape similarity with the natural hip bone. Thus, if $S_1' = \{I, III, V\}$ be the set of designs with high shape similarity from walking, and $S_2' = \{A, D\}$ be the set of designs with high shape similarity from sit-to-stand, then indiscriminate mixing gives $5! = 120$ permutations, while alternate selection of elements from S_1' and S_2' gives $2 \times 3! \times 2! = 24$ permutations. This intuitive user guided design approach leads to much saving in computation time as each optimization run takes approximately 8–9 h of computation time in a i7 3.60 GHz computer with 32 GB RAM.

3 Results

The section presents the optimal design of the hip bone for walking and sit-to-stand using a topology optimization solver (OptiStruct®). The simulations are performed on a desktop computer with an Intel(R) Core i7, 3.60 GHz processor and 32 GB of RAM that consumes approximately 8–9 h to converge to an optimal solution. This work uses isotropic elastic cortical bone properties (Young's

modulus = 17 GPa and Poisson's ratio = 0.3) in topology optimization and finite element analysis of the natural hip bone.

3.1 Optimal design of the hip bone for walking gait cycle

The optimal designs of the hip bone and the corresponding stress distributions for eight phases of walking are obtained from our previous work Kumar and Rakshit [25] and shown in Figs. 5 and 6, respectively. The first row gives the interior view, while the second row gives the exterior view of the optimal designs. The shape similarity values and compliance of the optimal designs are compared with the natural hip bone and listed in Table 5. Phases III and IV have high shape similarity with the natural hip bone since these two phases have inactive lower muscle forces, which creates a hole in the lower portion of the designs in the same region as the obturator foramen. Phase VI has high compliance (167 N-mm) and phase VII has low compliance (20.72 N-mm). Table 6 compares the maximum stress and maximum displacement of the optimally designed hip bones with the natural hip bone. Phase VI has high value of maximum stress (192.7 MPa) and phase II has low value of
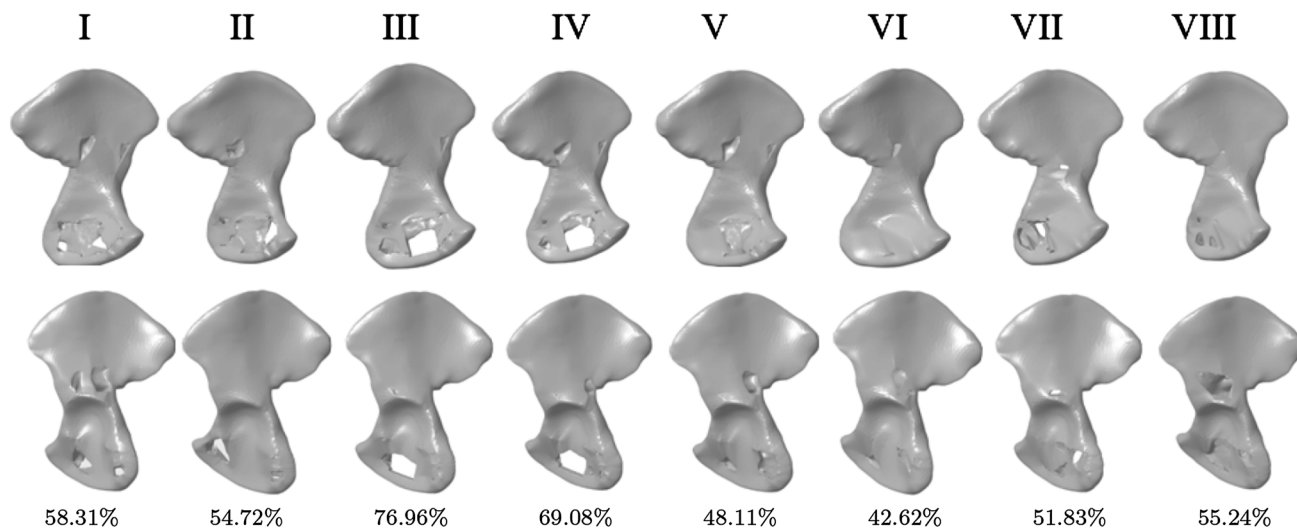
Fig. 5 Optimal designs of the hip bone for eight phases of walking gait cycle. The first row gives the interior view while the second row gives the exterior view of the optimal designs in each phase. At bottom the shape similarity values of the each optimal design with the natural hip bone are presented (adopted from [25])
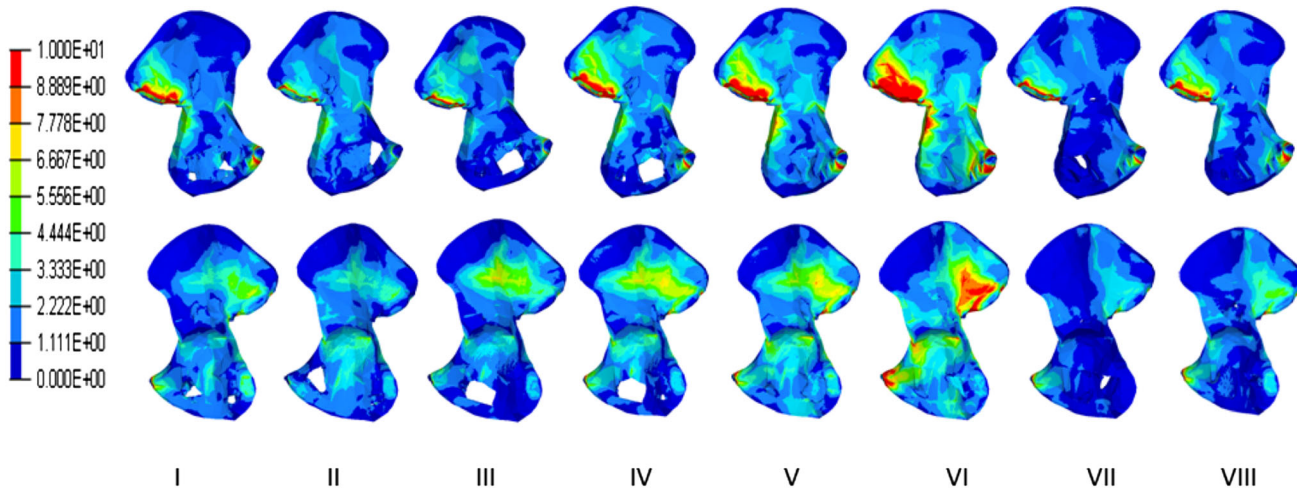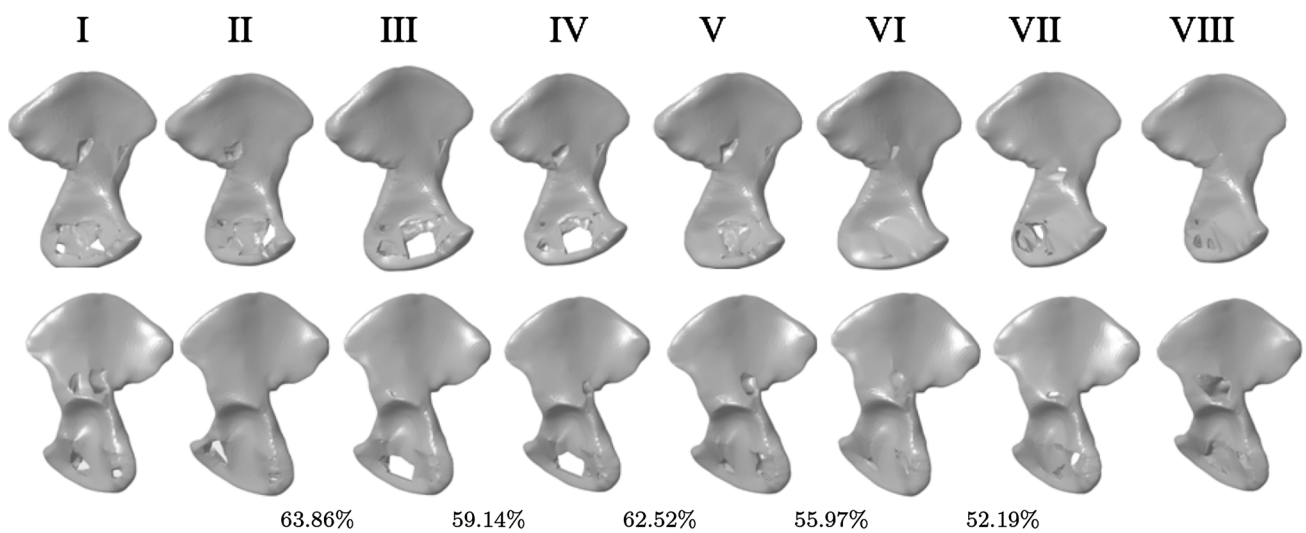

Fig. 6 von-Mises stress distribution of the optimal designs obtained from topology optimization for eight phases in a gait cycle. Top row represents the interior view and bottom row represents the exterior view. The values in legend are in MPa (adopted from [25])

Table 5 Shape similarity index and compliance of the optimal solution for eight phases of the gait cycle of a human weight 650 N

Phase	Shape similarity index (%)	Compliance of optimal design (N-mm)	Compliance of natural hip bone (N-mm)
I	58.31	50.85	58.35
II	54.72	26.70	30.47
III	76.96	31.90	33.43
IV	69.08	57.15	62.83
V	48.11	81.20	91.12
VI	42.62	167.58	196.04
VII	51.83	20.72	24.00
VIII	55.24	42.19	50.49

The value of initial shape similarity measurement is 46.13% (adopted from [25])

Table 6 Maximum stress and maximum displacement of the optimally designed hip bones and the natural hip bone during walking for a human of body weight of 650 N (adopted from [25])

Phase	Max. stress in optimal design (MPa)	Max. stress in natural hip bone (MPa)	Max. displacement in optimal design (mm)	Max. displacement in natural hip bone (mm)
I	92.35	94.24	0.178	0.189
II	40.79	41.45	0.102	0.089
III	72.73	73.47	0.174	0.175
IV	110.4	112.90	0.257	0.262
V	128.1	131.00	0.296	0.299
VI	192.7	200.00	0.419	0.437
VII	68.89	72.58	0.166	0.177
VIII	95.15	99.93	0.225	0.237

Fig. 7 Optimal designs of the hip bone for five phases of sit-to-stand. The first row gives the interior view while the second row gives the exterior view of the optimal designs in each phase. At bottom the shape similarity values of the each optimal design with the natural hip bone are presented

Fig. 8 von-Mises stress distribution of the optimal designs obtained from topology optimization for five phases of sit-to-stand. The top row represents the interior view and the bottom row represents the exterior view. The values in legend are in MPa
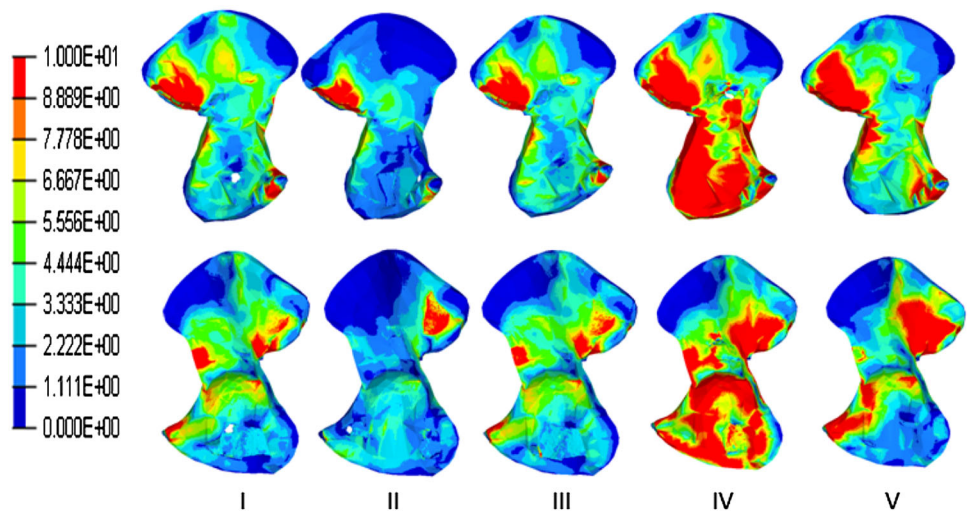
Table 7 Compliance and shape similarity index of the optimally designed hip bone and the natural hip bone during the sit-to-stand

Phase	Shape similarity index (%)	Compliance of Optimal design (N-mm)	Compliance of natural hip bone (N-mm)
I	63.86	130.28	165.75
II	59.14	64.9	82.17
III	62.52	127.12	161.97
IV	55.97	486.31	599.52
V	52.19	332.89	405.12

The value of initial shape similarity measurement is 46.13%

maximum stress (40.79 MPa). The highest value of maximum displacement is in phase VI (0.419 mm) and the lowest value of maximum displacement is in phase II (0.102 mm).

3.2 Optimal design of the hip bone for sit-to-stand

Figure 7 shows the optimal designs of the hip bone obtained for the five phases of the sit-to-stand and the corresponding stress distributions are shown in Fig. 8. Phases I and III create a small hole in the lower portion of the optimal designs, while the remaining phases only remove a layer of material from the lower portion. The size of the hole in the lower portion of sit-to-stand is small compared to walking as the high stresses in the lower portion of optimal designs of sit-to-stand are more than that of the optimal designs of walking (Figs. 6, 8). Table 7 lists the shape similarity values of the five optimal designs. Phase I has high shape similarity and is equal to 63.86%. The magnitude of lower muscles such as adductor muscles, semitendinosus, semimembranosus are low in the phases I and III. These muscles create low stresses in the lower portion and the hip joint force along with the upper muscles creates high stresses in the upper portion (Fig. 8). Hence, the material is removed from the lower portion and creates a hole similar to obturator foramen.

From Table 7 we see that the optimal designs have low compliance compared to the natural hip bone, which

indicates that the optimal designs are stiffer than the natural hip bone. Among all five phases, phase IV has high compliance (486.31 N-mm) and phase II has low compliance (64.90 N-mm). The maximum compliance value in walking is 196.04 N-mm, which is nearly 0.4 times the maximum compliance value of sit-to-stand. This is because of the high magnitude of the muscle forces in sit-to-stand than the walking. These muscle forces create high stresses in sit-to-stand as shown in Figs. 6 (vi) and 8 (iv). The number high stress zones are more in sit-to-stand than the walking, hence the high compliance in sit-to-stand. Table 8 enlists the maximum stress and maximum displacement of the optimal designs and the natural hip bone. Phase V has high value of maximum stress (308.5 MPa) and phase II has low values of maximum stress (97.05 MPa). The maximum stress value of walking (192.4 MPa) is nearly 0.6 times the maximum stress value of sit-to-stand as the magnitude of the muscles is high in sit-to-stand (Tables 2, 4). These phases also have high compliance values.

From Figs. 5 and 7, it is observed that not all phases create a hole in place of obturator foramen. Some phases of walking and sit-to-stand create a hole in lower portion, whereas the remaining phases remove material in upper portions as dents. Figure 5 shows that walking phases III and IV produce highest shape similarity by producing a moderate sized hole in the same region as the obturator foramen in the natural hip bone. Figure 6 shows in the corresponding stress plots that the lower portion in these

Table 8 Maximum stress and maximum displacement of the optimally designed hip bones and the natural hip bone during sit-to-stand for a human of body weight of 650 N

Phase	Max. stress in optimal design (MPa)	Max. stress in natural hip bone (MPa)	Max. displacement in optimal design (mm)	Max. displacement in natural hip bone (mm)
I	167.2	177.2	0.402	0.429
II	97.05	98.95	0.096	0.109
III	165.6	175.3	0.378	0.403
IV	307.0	320.1	0.623	0.678
V	308.5	324.8	0.659	0.707

phases is not highly stressed which may be the reason as to why the hole is generated in topology optimization. The holes generated in phases I and III of sit-to-stand are much smaller compared to that generated in walking. From Fig. 8 we notice that the stress ranges in phases I and III of sit-to-stand are similar to the stress ranges in phases III and IV in walking. However, in phases I and III of sit-to-stand the high and low stressed zones are sort of mixed (high stress red-green and low stress blue in Fig. 8) whereas in phases III and IV of walking there is clear demarcation between the high and low stressed zones (high stress green more in upper part and low stress blue in lower part in Fig. 6). Thus, we conclude that the lower part should not only experience low stress, but a contrasting stress profile, i.e., the upper part experiencing predominantly high stress and lower part predominantly low stressed, is an essential criterion for topology optimization to create a moderate sized hole in the same region as the obturator foramen.

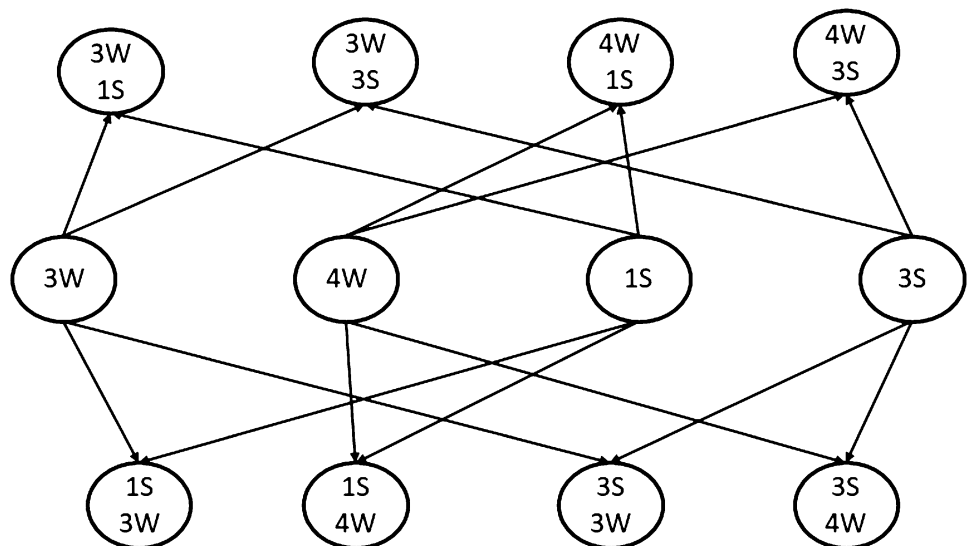### 3.3 Combination between sit-to-stand and walking

As explained before, each optimization run takes nearly 8–9 h on a desktop computer with 32 GB RAM and i7 3.60 GHz processor, considering all phases for combination of activity is computationally prohibitive. Hence, we choose two phases with high shape similarity from each ADL for the combination between walking and sit-to-stand. This reduces the total combinations to $2 \times 2! \times 2! = 8$. We select phase III and phase IV having shape similarity of 76.96% and 69.08%, respectively, from walking and phase I and phase III having shape similarity of 63.86% and 62.52%, respectively, from sit-to-stand for combination between walking and sit-to-stand. Figure 9 shows the list

of possible combinations between walking and sit-to-stand. The selected phases from the walking (3W, 4W) and sit-to-stand (1S, 3S) are shown in the middle row. As explained earlier, this gives a total of eight combinations and these eight combinations are divided into two sets based on the input and loading conditions. The first set consists of the first four combinations, where we apply walking loads on the modified input obtained from sit-to-stand and shown in last row of Fig. 9 with S-W sequence. The second set consists of the last four combinations, where we apply sit-to-stand loads on the modified input obtained from walking and shown in first row of Fig. 9 with W-S sequence. The following is a list of combinations of walking and sit-to-stand applied as put in the sequence:

- Case (i): phase I sit-to-stand and phase III walking (IS–IIIW)
- Case (ii): phase I sit-to-stand and phase IV walking (IS–IVW)
- Case (iii): phase III sit-to-stand and phase III walking (IIIS–IIIW)
- Case (iv): phase III sit-to-stand and phase IV walking (IIIS–IVW)
- Case (v): phase III walking and phase I sit-to-stand (IIIW–IS)
- Case (vi): phase III walking and phase III sit-to-stand (IIIW–IIIS)
- Case (vii): phase IV walking and phase I sit-to-stand (IVW–IS)
- Case (viii): phase IV walking and phase III sit-to-stand (IVW–IIIS)

Figure 10 explains the procedure of combination between walking and sit-to-stand by imposing phase I loads of sit-to-stand on optimal design obtained from phase III loads of walking. We observe that the optimization process

Fig. 9 The selected phases from the walking and sit-to-stand are shown in the middle row. The first and last rows give the eight possible combinations between walking and sit-to-stand
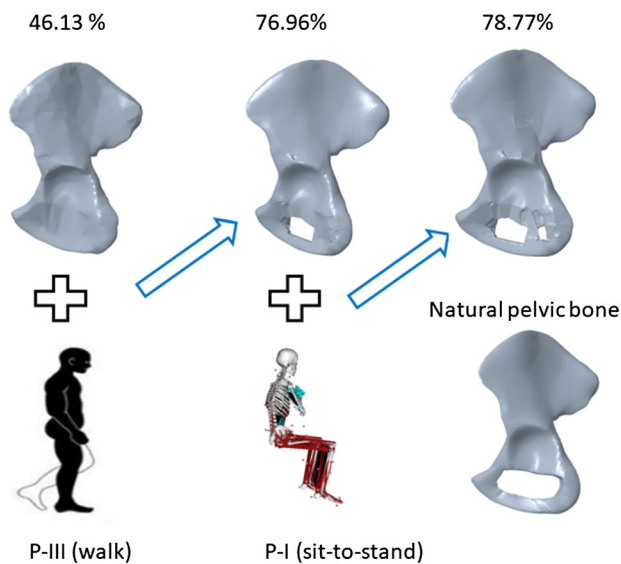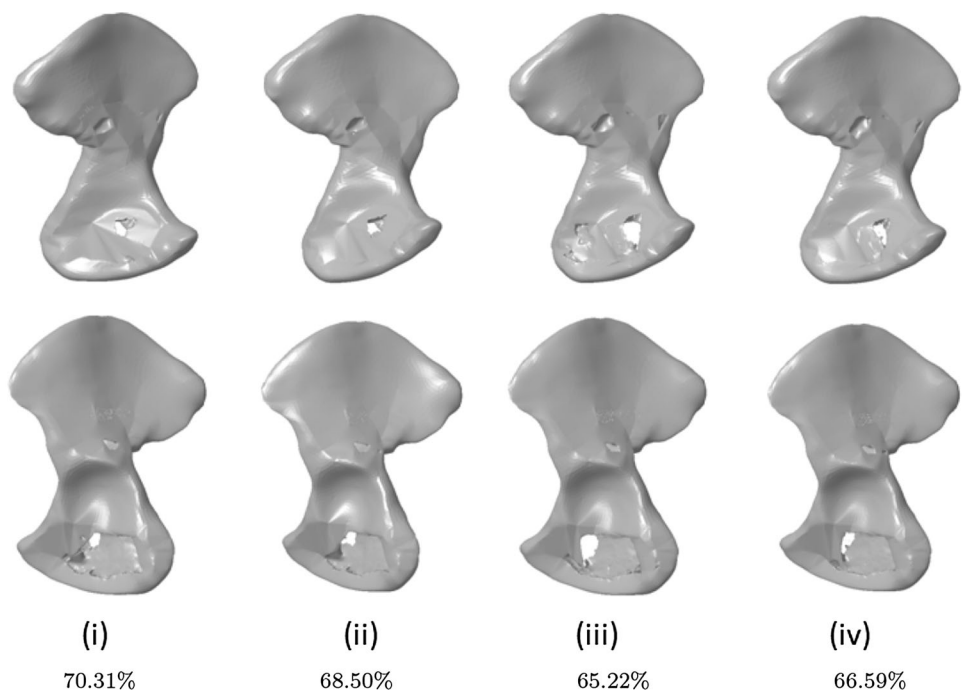
46.13 %   76.96%   78.77%

Natural pelvic bone

P-III (walk)   P-I (sit-to-stand)

Fig. 10 Schematic representation of the procedure of combination between walking and sit-to-stand by imposing phase I sit-to-stand loads on modified optimal design from phase III walking. The percentages above the figures indicate shape similarity with the natural hip bone

converges to a local optimal solution in 2-3 iterations. The obtained optimal design is similar to the input (the output from the phase III walking loads) because the input is already an optimal solution and optimization on this input does not give a better solution. So, we modify the input by patching the dents present in the upper portion which also has the effect of moving the initial input to the optimization solver sufficiently away from the local minimum

corresponding to the previous solution. This procedure is done for all eight combinations to give enough deviation to the optimization solver to converge to different distinct optimal solutions. This procedure also ensures wide-range exploration of the multi-dimensional design space.

3.3.1 Combination of sit-to-stand and walking

This section presents the optimal design of the hip bone obtained from applying walking loads of phases III and IV on the optimal designs from sit-to-stand of phases I and III. The four combinations are:

- Case (i): IS–IIIW
- Case (ii): IS–IVW
- Case (iii): IIIS–IIIW
- Case (iv): IIIS–IV W

Figure 11 shows the four optimal designs obtained from the combination of sit-to-stand and walking phases, i.e., applying the walking loads on the modified input obtained from the sit-to-stand and the corresponding stress distributions are shown in Fig. 12. Table 9 presents the shape similarity values and compliance of the four optimal designs. Case (i) has high shape similarity due to the presence of a small hole and surface dents in the upper portion of the design. Although the size of the hole in the case (iii) is bigger than the other optimal designs, presence of surface dents in both lower and upper portion causes low shape similarity. Phases III and IV of walking remove material from lower portion of design since the lower
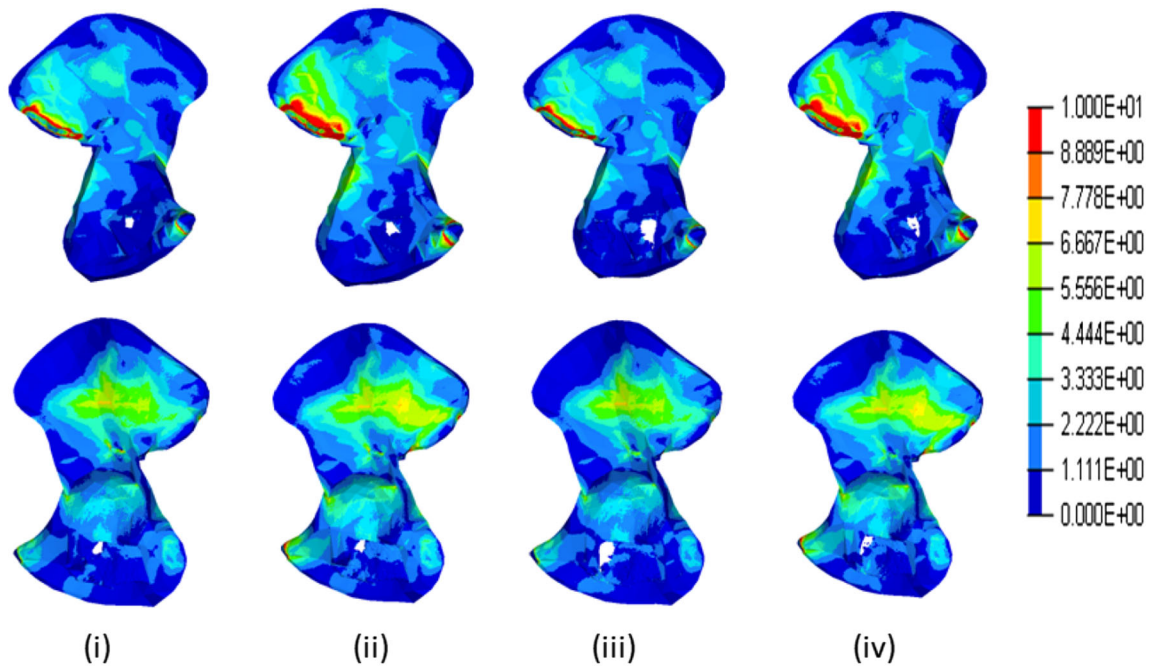
Fig. 11 Optimal designs of the hip bone obtained by imposing walking load conditions on the modified input from the sit-to-stand. At bottom the shape similarity values of the each optimal design with the natural hip bone are presented

(i)   (ii)   (iii)   (iv)
70.31%   68.50%   65.22%   66.59%

Fig. 12 von-Mises stress distribution of the optimal designs obtained from the combination of sit-to-stand and walking. The values in legend are in MPa

Table 9 Compliance and shape similarity values of optimal designs obtained from the combination of sit-to-stand and walking

Case	Shape similarity index (%)	Compliance of optimal design (N-mm)	Compliance of natural hip bone (N-mm)
i	70.31	30.03	33.43
ii	68.50	58.86	62.83
iii	65.22	29.81	33.43
iv	66.59	58.55	62.83

muscles creates less stresses in the lower portion than the upper portion (Fig. 12). But in the above optimal designs, these loads create a tiny hole and keep a layer of material in the lower portion of the design. This is due to the inputs which are obtained from the sit-to-stand have a hole in the upper portion. Hence, the loads do not create a complete hole to preserve the volume constraint. In summary, the shape similarity increased with respect to sit-to-stand

optimal designs, but reduced with respect to optimal designs from walking. Case (iii) has the lowest value of compliance (29.81 N-mm), whereas case (ii) has highest value of compliance (58.86 N-mm). Case (i) and case (iii) have low compliance than case (ii) and case (iv) since phase IV walking produces high compliance compared to phase III walking. Case (ii) and case (iv) designs have more

Table 10 Maximum stress and maximum displacement of the optimally designed hip bones from the combination of sit-to-stand and walking and the natural hip bone for a human of body weight of 650 N

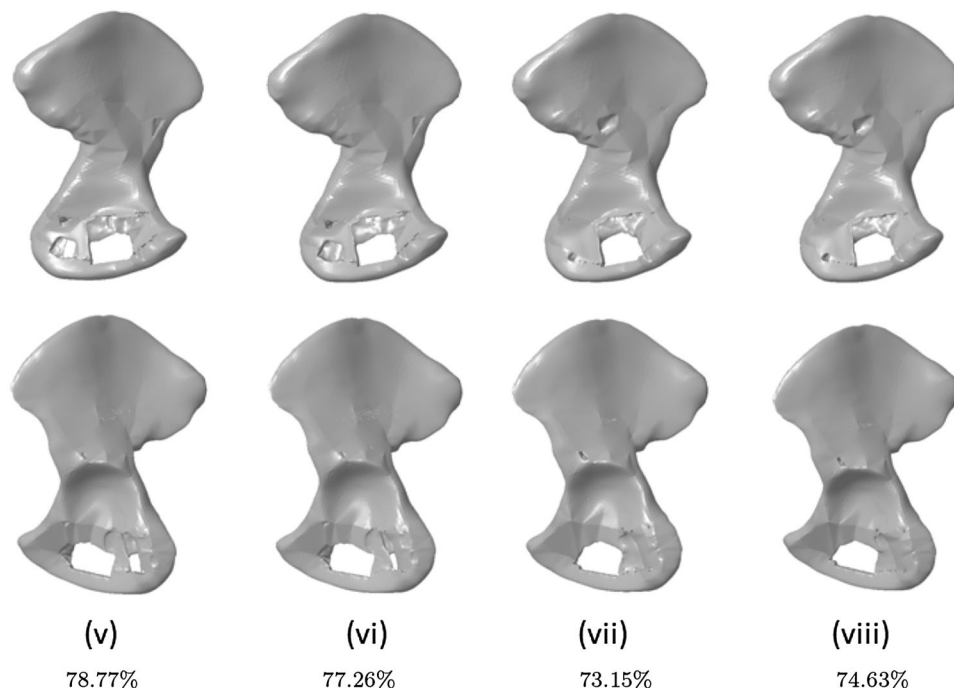| Case	Max. stress in optimal design (MPa)	Max. stress in natural hip bone (MPa)	Max. displacement in optimal design (mm)	Max. displacement in natural hip bone (mm)
i	72.44	73.47	0.164	0.175
ii	110.2	112.90	0.243	0.262
iii	72.83	73.47	0.166	0.175
iv	109.8	112.90	0.241	0.262

Fig. 13 Optimal designs of the hip bone obtained by imposing sit-to-stand load conditions on the modified input from the walking. The top row gives the interior view and the bottom row gives the exterior view. At bottom the shape similarity values of the each optimal design with the natural hip bone are presented

high-stress zones (red colour zones above 10 MPa in Fig. 12) implies high compliance than the other two cases.

Table 10 presents the maximum stress of optimal designs from cases (i)–(iv) and the natural hip bone. It is observed that the maximum stress of the optimal designs is closely matched with the natural hip bone. Case (ii) design has the highest value of maximum stress and is equal to 110.2 MPa, whereas case (i) has the lowest value of maximum stress and is equal to 72.44 MPa. Table 10 also enlists the maximum displacement value of optimal designs and natural hip bone. It is clear that the maximum displacement are lower in optimal design compared to natural hip bone. The highest value of maximum displacement occurs in case (ii) and is equal to 0.243 mm, whereas the lowest value occurs in case (i) and is equal to 0.164 mm.

3.3.2 Combination of walking and sit-to-stand

This section presents the optimal design of the hip bone obtained from applying sit-to-stand loads of phases I and III on the optimal designs from walking of phases III and IV. The four combinations are:

- Case (v): IIIW–IS
- Case (vi): IIIW–IIIS
- Case (vii): IVW–IS
- Case (viii): IVW–IIIS

Figure 13 shows the optimal designs obtained from the combination of walking and sit-to-stand, i.e., applying loads of sit-to-stand on the optimal designs obtained from the walking. The shape similarity values and compliance of all four designs are presented in Table 11. Case (v) design has highest shape similarity and is equal to 78.77%.

Table 11 Compliance and shape similarity values of optimal designs obtained from combination of walking and sit-to-stand

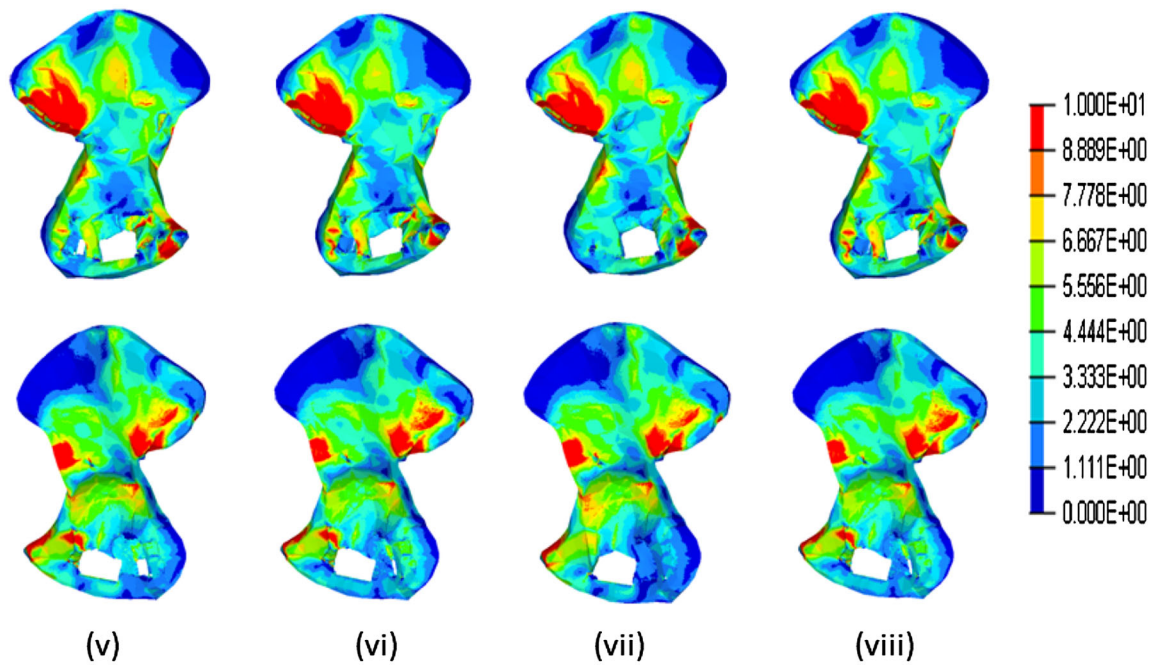| Case	Shape similarity index (%)	Compliance of Optimal design (N-mm)	Compliance of natural hip bone (N-mm)
v	78.77	155.31	165.75
vi	77.26	149.48	161.97
vii	73.15	154.34	165.75
viii	74.63	148.69	161.97

Fig. 14 von-Mises stress distribution of the four optimal designs obtained by imposing sit-to-stand loads on the modified input from the walking. The values in legend are in MPa

Table 12 Maximum stress and maximum displacement of the optimally designed hip bones from the combination of walking and sit-to-stand and the natural hip bone for a human of body weight of 650 N

Case	Max. stress in optimal design (MPa)	Max. stress in natural hip bone (MPa)	Max. displacement in optimal design (mm)	Max. displacement in natural hip bone (mm)
v	172.2	177.2	0.417	0.429
vi	170.4	175.3	0.391	0.403
vii	169.0	177.2	0.410	0.429
viii	167.5	175.3	0.386	0.403

Table 13 Comparison of compliance, shape similarity, max. stress and max. displacement values for the optimal design with buttress (Fig. 13 (v)) and without buttress (Fig. 15) in the lower portion

Quantity	Natural hip bone	with buttress (Fig. 13 (v))	without buttress (Fig. 15)
Compliance (N-mm)	165.75	155.31	159.20
Shape similarity (%)	100	78.77	81.85
Max. stress (MPa)	177.2	172.2	173.6
Max. displacement (mm)	0.429	0.417	0.426
Volume (mm^3)	259,808	259,355	258,362

Although two holes are generated (a large one and a smaller one), the enhanced similarity is probably due to overall shape similarity of the zone close to the obturator foramen. The optimal designs obtained from the combination of walking and sit-to-stand have high shape similarity than the optimal designs from the combination of sit-to-stand and walking. This indicates that the final design is dependent not only on the selection of the particular phases, but also on the sequence in which they are applied. Table 11 also presents the compliance of both the optimal designs obtained from combination of walking and sit-to-stand and the natural hip bone. Case (viii) has the lowest
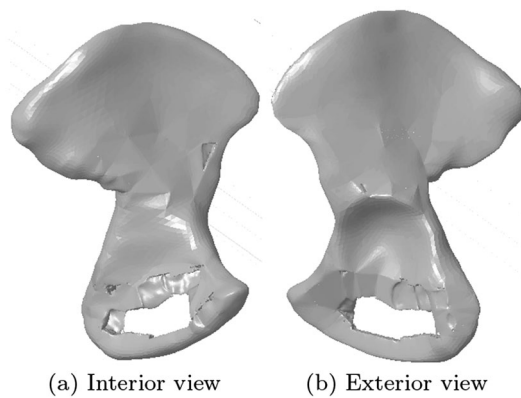
(a) Interior view   (b) Exterior view

Fig. 15 Optimal design after removing the buttress from lower portion of the optimal design obtained from case (v) (Fig. 13 (v))
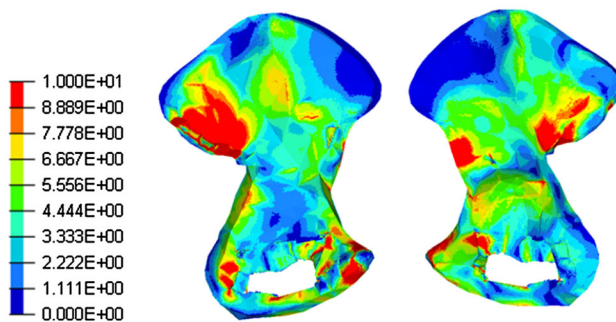

Fig. 16 von-Mises stress distribution of the optimal design after removing the buttress from case(v) (Fig. 13 (v)). The values in legend are in MPa

value of compliance (148.69 N-mm), whereas case (v) has highest value of compliance (155.31 N-mm). Case (v) and case (vii) have higher value of compliance than case (vi) and case (viii) since phase I of sit-to-stand generates higher compliance than phase III of sit-to-stand. The optimal designs obtained from the combination of walking and sit-to-stand have high compliance than the optimal designs obtained from the combination of sit-to-stand and walking. Since phases I and III of sit-to-stand have high muscle activity than phases III and IV of walking, which produces high stresses in sit-to-stand. Optimal designs from the sequence walking first, and then sit-to-stand produces higher shape similarity than sit-to-stand first, then walking. It is also interesting to note that once the hole is created in the zone of the obturator foramen, other loading conditions only enlarge the hole in that zone.

Figure 14 shows the von-Mises stress distribution of the four optimal designs. High-stress zones are presented in the upper portion of the hip bone near the acetabulum, the pubis bone and around the acetabulum. Sacro-iliac joint and pubic symphysis experiences the maximum stress. The

stress distribution of the four optimal design are almost similar since the muscle forces of phase I and phase III loads follow the same trend. This can be the reason for closest values for compliance (maximum is 155.31 N-mm and 148.69 N-mm) of the four optimal designs. Table 12 lists maximum stress values of optimal designs and natural hip bone. The highest value of maximum stress is in case (v) and is equal to 172.2 MPa, whereas the lowest value of maximum stress is in case (viii) and is equal to 167.5 MPa. It is observed that the maximum stress is low in optimal designs compared to natural hip bone. Table 12 also enlists the maximum displacements of optimal design and natural hip bone. The highest value of maximum displacement is in case (v) and is equal to 0.417 mm, whereas the lowest value is in case (viii) and is equal to 0.386 mm (Table 13).

3.3.3 User-guided prosthesis design

We observe two holes in lower portion of optimal design obtained from case (v) and case (vi) (Fig. 13 (v) and (vi) respectively) and the part between the holes looks like a buttress. However, such a buttress may cause obstruction of the blood vessels and nerves that pass through the obturator foramen. From a prosthesis point of view also such a part might be difficult to manufacture and form a weak link in the final product. Hence, a designer may wish to remove this buttress from the final design if it does not lead to much change in compliance and maximum stress. To see the effect, we remove the buttress from case (v) design. Figure 15 shows the design after removing the buttress. The shape similarity of the design increases to 81.85% from 78.77%. The compliance value is 159.2 N-mm which is higher than compliance value of 155.31 N-mm of the optimal design from which the new design is derived, but lower than the compliance value of 165.75 N-mm of the natural hip bone. Figure 16 shows the stress distribution of the design. The variation of compliance due to the buttress removal is 2.5%, while for the stress it is equal to 0.81%. Thus, this design may be accepted as the best design with highest shape similarity and higher stiffness than the natural hip bone.

4 Conclusions and future work

In this work, we explored whether loads from ADLs can form a structure similar in geometry to the hip bone under the same structural and functional constraints as the natural hip bone. This is posed as a compliance minimization problem under loads of two ADLs, walking and sit-to-stand, along with the volume constraint equal to the volume of the natural hip bone and solved using the topology

optimization software OptiStruct®. The current work is the first attempt to design hip bone for sit-to-stand motion. The optimal designs are compared for shape similarity with the natural hip bone using Procrustes analysis. We also developed a two-step user guided design approach in which final designs are arrived after application of loads of one ADL on the optimal designs obtained from the other ADL. The current work is an initial work to design the hip bone using the above discussed two-step approach. Our results show that we can achieve structures stiffer than the natural hip bone while maintaining good shape similarity with the same.

As mentioned before, this is one of the first works on designing the global geometry of a complex structure like the hip bone using topology optimization. The results can be validated by conducting experiments on the obtained optimal designs and natural hip bone for simple boundary conditions. This work can be extended to other human activities like stair climbing, running, cycling, etc. In the present work, we used cortical bone properties to design the hip bone since the OptiStruct® solver is not able to design sandwich material, hence one can extend this work to design of sandwich materials. Then, the research work will comprise both design of bone micro-structure and optimization of global geometry of the hip bone.

Nature performs a multi-criterion optimization (objectives like metabolic cost, time varying functions), to arrive the current shape of the hip bone. However, in the current work, we have done single objective optimization. Other types of objectives can be included to extend the current work. This work can be extended to include the constraints related to obstruction of the blood vessels and nerves while doing topology optimization.

This work is the first step towards the design of prosthesis including the effect of muscle forces using topology optimization. It is identified that the mass of the prosthesis and natural hip bone is not same due to different material properties. One can include a mass constraint while designing the prosthesis to reduce the mass of it. Further, the mass of the prosthesis can be reduced by using lattice-structured material instead of a solid material.

Compliance with ethical standards

Conflicts of interest The authors declare that they have no conflict of interests.

References

1. Haq, R., Srivastava, A., Dhammi, I.: Classification of pelvic fractures and its clinical relevance. J. Orthop. Traumatol. Rehab. **7**(1), 8–13 (2014)
2. Goel, V.K., Svensson, N.L.: Forces on the pelvis. J. Biomech. **10**(3), 195–200 (1977)
3. Goel, V.K., Valliappan, S., Svensson, N.L.: Stresses in the normal pelvis. Comput. Biol. Med. **8**(2), 91–104 (1978)
4. Dostal, W.F., Andrews, J.G.: A three dimensional biomechanical model of hip musculature. J. Biomech. **14**(11), 803–812 (1981)
5. Bergmann, G., Graichen, F., Rohlmann, A.: Hip joint loading during walking and running, measured in two patients. J. Biomech. **26**(8), 969–990 (1993)
6. Dalstra, M., Huiskes, R.: Load transfer across the pelvic bone. J. Biomech. **28**(6), 715–724 (1995)
7. Anderson, A.E., Peters, C.L., Tuttle, B.D., Weiss, J.A.: Subject-specific finite element model of the pelvis: development, validation and sensitivity studies. J. Biomech. Eng. **127**(3), 364–373 (2005)
8. Ghosh, R., Mukherjee, K., Gupta, S.: Bone remodelling around uncemented metallic and ceramic acetabular components. Proc. Inst. Mech. Eng. [H] **227**(5), 490–502 (2013)
9. Ghosh, R., Pal, B., Ghosh, D., Gupta, S.: Finite element analysis of a hemi-pelvis: the effect of inclusion of cartilage layer on acetabular stresses and strain. Comput. Methods Biomech. Biomed. Eng. **18**(7), 697–710 (2015)
10. Mukherjee, K., Gupta, S.: Bone ingrowth around porous-coated acetabular implant: a three-dimensional finite element study using mechanoregulatory algorithm. Biomech. Model. Mechanobiol. **15**(2), 389–403 (2016)
11. Hu, P., Wu, T., Wang, H.Z., Qi, X.Z., Yao, J., Cheng, X.D., Chen, W., Zhang, Y.Z.: Influence of different boundary conditions in finite element analysis on pelvic biomechanical load transmission. Orthop. Surg. **9**(1), 115–122 (2017)
12. Ricci, P.L., Maas, S., Kelm, J., Gerich, T.: Finite element analysis of the pelvis including gait muscle forces: an investigation into the effect of rami fractures on load transmission. J. Exp. Orthop. **5**(1), 1–9 (2018)
13. Ramezani, M., Klima, S., De La Herverie, P.L.C., Campo, J., Le Joncour, J.B., Rouquette, C., Scholze, M., Hammer, N.: In silico pelvis and sacroiliac joint motion: refining a model of the human osteoligamentous pelvis for assessing physiological load deformation using an inverted validation approach. BioMed Res. Int. **2019**, 1 (2019)
14. Millington, P.J., Myklebust, B.M., Shambes, G.M.: Biomechanical analysis of the sit-to-stand motion in elderly persons. Arch. Phys. Med. Rehab. **73**(7), 609–617 (1992)
15. Kotake, T., Dohi, N., Kajiwara, T., Sumi, N., Koyama, Y., Miura, T.: An analysis of sit-to-stand movements. Arch. Phys. Med. Rehab. **74**(10), 1095–1099 (1993)
16. Mourey, F., Grishin, A., D'Athis, P., Pozzo, T., Stapley, P.: Standing up from a chair as a dynamic equilibrium task: a comparison between young and elderly subjects. J. Gerontol. Ser. A Biol. Sci. Med. Sci. **55**(9), 425–431 (2000)
17. Janssen, W.G., Bussmann, H.B., Stam, H.J.: Determinants of the sit-to-stand movement: a review. Phys. Ther. **82**(9), 866–879 (2002)
18. Yoshioka, S., Nagano, A., Hay, D.C., Fukashiro, S.: Peak hip and knee joint moments during a sit-to-stand movement are invariant to the change of seat height within the range of low to normal seat height. BioMed. Eng. Online **13**(1), 1–13 (2014)
19. Caruthers, E.J., Thompson, J.A., Chaudhari, A.M., Schmitt, L.C., Best, T.M., Saul, K.R., Siston, R.A.: Muscle forces and their contributions to vertical and horizontal acceleration of the Center

of mass during sit-to-stand transfer in young, healthy adults. J. Appl. Biomech. **32**(5), 487–503 (2016)

20. Tse, K.M., Lee Robinson, D., Franklyn, M., Zhang, J.Y., Spratley, E.M., Salzar, R.S., Fernandez, J., Ackland, D.C., Lee, P.V.S.: Effect of sitting posture on pelvic injury risk under vertical loading. J. Mech. Behav. Biomed. Mater. **108**, 103780 (2020)

21. Fernandes, P., Rodrigues, H., Jacobs, C.: A model of bone adaptation using a global optimisation criterion based on the trajectorial theory of wolff. Comput. Methods Biomech. Biomed. Eng. **2**(2), 125–138 (1999)

22. Fernandes, P.R., Folgado, J., Jacobs, C., Pellegrini, V.: A contact model with ingrowth control for bone remodelling around cementless stems. J. Biomech. **35**(2), 167–176 (2002)

23. Lekszycki, T.: Optimality conditions in modeling of bone adaptation phenomenon. J. Theor. Appl. Mech. **37**(3), 607–624 (1999)

24. Lekszycki, T.: Modelling of bone adaptation based on an optimal response hypothesis. Meccanica **37**(4–5), 343–354 (2002)

25. Kumar, K.E.S., Rakshit, S.: Topology optimization of the hip bone for gait cycle. Struct. Multidiscip. Optim. **62**(4), 2035–2049 (2020)

26. Kumar, K.E.S., Rakshit, S.: Topology optimization of the hip bone for walking using multi-load approach. In: International Mechanical Engineering Congress & Exposition. ASME (2020)

27. Kumar, K.E.S., Rakshit, S.: Topology optimization of the pelvic bone prosthesis under single leg stance. In: Volume 11B: 46th Design Automation Conference (DAC), International Design Engineering Technical Conferences and Computers and Information in Engineering Conference, V11BT11A030 (2020)

28. Bendsøe, M.P., Sigmund, O.: Topology optimization: theory, methods and applications, 2nd edn. Springer, London (2004)

29. Rozvany, G.: The simp method in topology optimization—theoretical background, advantages and new applications. In: Proceedings of 8th AIAA/USAF/NASA/ISSMO Symposium on Multidisciplinary Analysis and Optimization (2000)

30. Sigmund, O., Maute, K.: Topology optimization approaches: a comparative review. Struct. Multidiscip. Optim. **48**(6), 1031–1055 (2013)

31. Phillips, A.T., Villette, C.C., Modenese, L.: Femoral bone mesoscale structural architecture prediction using musculoskeletal and finite element modelling. Int. Biomech. **2**(1), 43–61 (2015)

32. Van Arkel, R.J., Modenese, L., Phillips, A.T., Jeffers, J.R.: Hip abduction can prevent posterior edge loading of hip replacements. J. Orthop. Res. **31**(8), 1172–1179 (2013)